



# Pattern Diversity Based Four-Element Dual-band MIMO Patch Antenna for 5G mmWave Communication Networks

Waleed Tariq Sethi<sup>1</sup> · Saad Hassan Kiani<sup>2</sup> · Mehre E. Munir<sup>3</sup> ·  
Daniyal Ali Sehrai<sup>4,6</sup> · Huseyin şerif savci<sup>2</sup> · Dawar Awan<sup>5</sup>

Received: 7 February 2024 / Accepted: 17 April 2024 / Published online: 10 May 2024  
© The Author(s) 2024

## Abstract

This study presents a planar dual-band multiple-input multiple-output (MIMO) antenna design for the prospective fifth-generation (5G) frequency bands of 28 and 38 GHz. The antenna element is designed by utilizing a rectangular patch with an offset microstrip feeding technique. A dual-band response is achieved by placing semi-circular slots on each side of the patch element. To tune the frequency response and improve impedance matching, vertical rectangular slits are etched in the rectangular patch and the ground plane, respectively. The results show that the single antenna element offers an impedance bandwidth of 2.52 GHz (26.32–28.84 GHz) and 7.5 GHz (34–41.5 GHz). In addition, a MIMO configuration based on pattern diversity using four antenna elements is designed and fabricated. The designed MIMO configuration achieves an impedance bandwidth of 3 GHz (27–30 GHz) and 5.46 GHz (35.54–41 GHz) at operating bands of 28 and 38 GHz. The peak realized gain for the single element at 28 and 38 GHz is noted to be 7.4 dBi and 7.5 dBi, respectively. Furthermore, the polarization diversity configuration illustrates an isolation of > 15 dB and > 25 dB for the 28 and 38 GHz frequency bands, respectively. Moreover, the MIMO configuration attains appropriate values for the envelope correlation coefficient (ECC) and diversity gain (DG), Total Active Reflection Co-efficient (TARC), Channel Capacity Loss (CCL) and Mean Effective Gain (MEG) for the operating frequency bands. The proposed MIMO system based on results seems to be potential choice for mmwave Ka Band Applications.

**Keywords** Dual-band · Fifth generation · MIMO · Planar antenna · Pattern diversity

## 1 Introduction

Fifth Generation (5G) technology has gathered significant attention from researchers, propelled by the relentless pursuit of enhancing both infrastructure construction and terminal installations. This heightened interest stems from the

continuous exploration and refinement aimed at bolstering the capabilities of 5G networks, fostering a landscape where faster data speeds, lower latency, and increased connectivity are not only sought after but also imperative for meeting the evolving demands of our interconnected world [1]. 5G technology currently uses lower frequencies (sub-6 GHz) for wide-area coverage, while higher frequencies, or millimeter-wave (mmWave) bands, are still being developed for local area networks and short-range indoor communications [2, 3]. Because of its broadband and consequent ability to provide multigigabits per second data speed, the intended exploitation of the mmWave band will unquestionably boost the efficient communication experience compared to the sub-6 GHz band [4, 5]. To build their own standards, many nations have chosen specific frequencies for 5G mmWave applications, such as 27.5–28.8 GHz for Japan, 28 GHz for Korea, and 24.2–27.5 GHz/37–43.5 GHz for China [6]. In October 2015, the Federal Communications Commission (FCC) suggested a careful examination of the spectrum at 28 GHz, 37 GHz, 39 GHz, and 64–71 GHz. Therefore, devices for these bands are essential for 5G communication systems [7, 8].

The mmWave antenna design faces significant challenges, primarily focusing on bandwidth enhancement and size reduction while maintaining low profile, multiple resonance capabilities, and cost-effectiveness. Adhering to international standards for the mmWave band, the adoption of dual-band realization is prevalent, offering advantages such as improved signal strength, reliability amidst interference, expanded coverage in challenging terrain, and reduced interference through separate frequency bands. Dual-band antennas contribute significantly to enhancing the performance and reliability of wireless communication systems, making them indispensable in modern communication technology. In mmwave spectrum, Intelligent Reflective Surfaces (IRS) hold immense potential. In IRS through deploying reflective surfaces can overcome fading effects hurdles effectively. By manipulating and redirecting mmWave signals, IRS optimizes their propagation, extending coverage and enhancing signal strength. However, IRS technology can be expensive, particularly in large-scale deployments where numerous reflective elements are required. This cost may pose a barrier to widespread adoption, especially for smaller operators or in resource-constrained environments [9–11]. In [12] authors presented an IMS-based pattern and beam reconfigurable antenna designed for diverse IoT applications, including V2X communication and 5G Small Cell deployment, both indoors and outdoors. This antenna system combines a wideband monopole with a programmable IMS acting as a reflector, offering versatility in radiation pattern control. Utilizing a single-layered metasurface comprising a  $4 \times 4$  array of square ring-shaped unit cells, each controllable by four diodes, the system enables precise manipulation of the reflector's shape and size, resulting in various radiation patterns from omnidirectional to broadside, with single or dual beams and beam-steering capabilities in both elevation and azimuth planes. Despite its advantages, challenges such as complexity in design and calibration, power consumption due to active components, and potential high costs associated with sophisticated IMS technology remain to be addressed for wider practical adoption in IoT and 5G applications.

Despite its appealing features, 5G faces a significant drawback of signal weakening during transmission due to low penetration power. To address this, multiple-input multiple-output (MIMO) technology is crucial, enhancing data rates and communication quality by increasing antenna components on transmitters and receivers. Efforts have been made to enhance radiation performance and propose metrics for 5G massive MIMO mmWave antennas. In [13], the authors used a complex multilayer substrate integrated waveguide (SIW) transmission line-fed coupling-based technology to get MIMO characteristics at 28 and 38 GHz frequency bands. Similarly, in [14], a dual-band MIMO antenna was designed for the microwave and mmWave bands by utilizing SIW aperture-based technology. Multilayer adaptation was used to achieve a wide impedance bandwidth with minimal coupling loss. The authors in [15] achieved dual-band resonance in the mmWave band by using LTCC-based technology. A 45°-polarized patch antenna fed by two pairs of differential L-type probes was used to implement the filtering antenna element. Each probe was coupled to an additional square ring and open strips, which produced radiation nulls and achieved a low and high stopband rejection level of > 24 dB with excellent selectivity. Resonant cavity antenna (RCA) technology was used by the authors in [16] to attain a high gain. To cover the 28 and 38 GHz frequency bands, the heights of the second- and third-order resonances in the RCA were optimized. Stepped rings were added to the metal ground, and a circular patch was applied to a partially reflecting surface (PRS) to increase the bandwidth and gain in both bands. In a nutshell, MIMO technology has many benefits, but it also offers many challenges. To achieve the best performance, several MIMO performance parameters must be optimized.

The presented literature study suggests that at the 28 and 38 GHz mmWave frequency bands, many researchers present phenomenal work, but it lacks simplicity as most of the discussed literature worked on utilizing multilayer designs, LTCC technology, and SIW-based structures that require precise alignments during fabrication, high costs of materials and adhesives, and time consumption due to multiple fabrication trials. To cater to this problem of multilayer designs and costly materials, in this paper, a novel planar dual-band antenna intended for operation at the 28 and 38 GHz mmWave frequency bands is presented. Notable contributions and objectives of the proposed work are as follows:

- The primary objective is to design a cost-effective planar structure that offers a novel design and can resonate at the mmWave frequency bands, i.e., 28 and 38 GHz.
- The proposed single-element design utilizes semi-circular slots on the edges of the radiating patch and slots on the radiating structure and ground plane to achieve an impedance bandwidth of 2.52 GHz (26.32–28.84 GHz) and 7.5 GHz (34–41.5 GHz).
- Pattern diversity configuration is utilized for the MIMO antenna design that exhibits an impedance bandwidth of 3 GHz and 5.46 GHz at the bands of interest.
- The isolation between the antenna elements is noted to be > 15 dB and > 25 dB at 28 and 38 GHz, respectively.

- The single element of the MIMO configuration achieved a realized gain of 7.4 and 7.5 dBi at 28 and 38 GHz, respectively.

## 2 Proposed Antenna Design

### 2.1 Single Antenna Element

Before presenting the design of a four-element MIMO antenna, there is a need to discuss the design of a single antenna element and its working principle. The geometry of the proposed dual-band antenna is shown in Fig. 1. The proposed antenna is printed on a low-loss Rogers RT-5880 substrate with a height ( $h$ ) of 0.787 mm and a dielectric constant ( $\epsilon_r$ ) of 2.2. It is composed of a modified rectangular patch element fed by an offset microstrip feed line.

The dual-band response is achieved by placing semi-circular slots on each side of the rectangular patch. Furthermore, to achieve maximum impedance matching at the desired frequency bands, rectangular slots of different dimensions are etched from the rectangular patch and the full ground plane, as shown in Fig. 1. The design process for the proposed dual-band antenna is shown in Fig. 2. In the first step, a conventional rectangular patch antenna is designed and analyzed, as shown in the inset of Fig. 2a. The results show that the conventional patch antenna provides resonance around 28.5 GHz. In the second step, the position of the microstrip feed line is changed (see inset of Fig. 2a). This modification tends to achieve a dual-band response, but the lower frequency band shifts below 26 GHz, as shown in Fig. 2. To tune the frequency response of the antenna at the desired bands, semi-circular slots are etched from each side of the patch element, as shown in the inset of Fig. 2. The utilization of semi-circular slots helps to achieve resonance at the desired frequency bands (see Fig. 2). In the last step, for improved impedance matching, vertical rectangular slots are etched from the rectangular patch and the ground plane, as shown

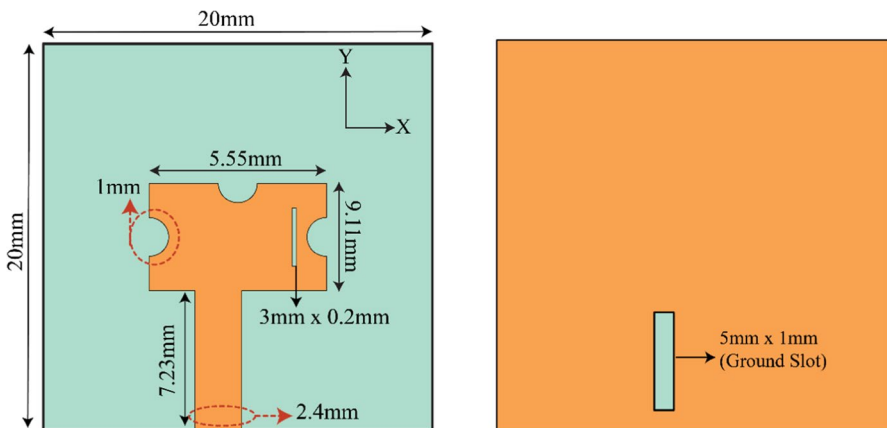
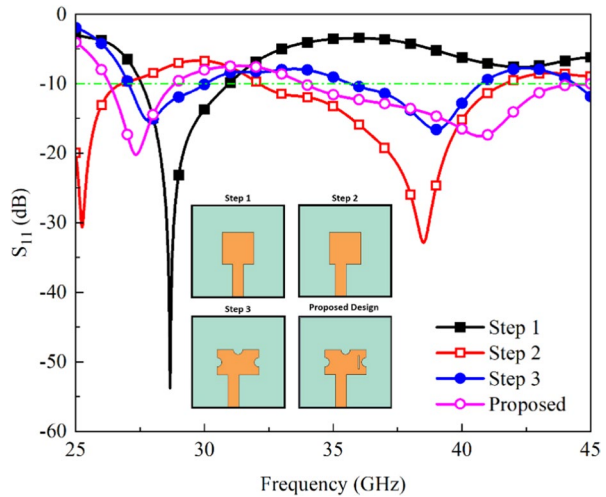


Fig. 1 Geometry of the proposed dual-band patch antenna (a) Front (b) Back

**Fig. 2 (a)** Reflection coefficient ( $S_{11}$ ) response for different design stages (inset of the figure shows design evolution)



in the inset of Fig. 2. From Fig. 2, one can observe that the use of slots in the radiating element and the ground plane improves the impedance matching at the 28 and 38 GHz frequency bands. The impedance bandwidth of the proposed design is noted to be 2.52 GHz (26.32–28.84 GHz) and 7.5 GHz (34–41.5 GHz).

Figure 3 illustrates the surface current distributions at resonance frequencies of 28 and 38 GHz. The surface current indicates that the dual resonances are generated through the combined effects of slots and semi-circles. Notably, there is a pronounced and constructive concentration of current along all semi-circles and the slot patch. Interestingly, at 38 GHz, the current is particularly pronounced on the left side of the radiating element.

The results of the parametric analysis for the proposed mmWave antenna are depicted in Fig. 4. This analysis specifically explores the effects of variations in

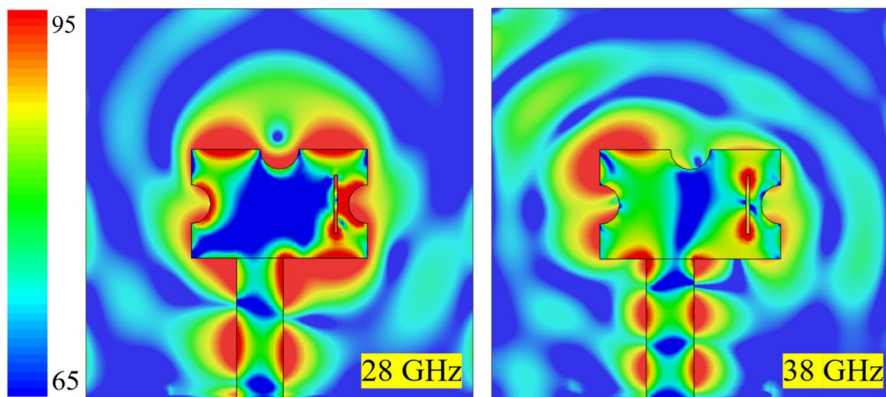


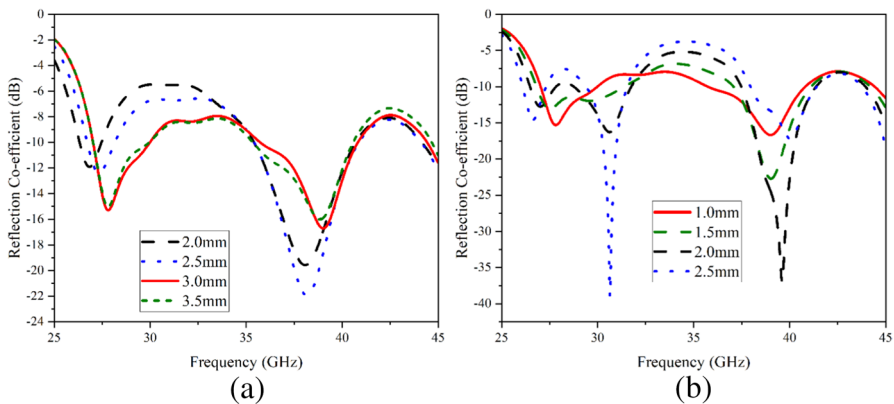
**Fig. 3** Surface current distribution at 28 and 38 GHz

patch slot length and ground slot width. Looking at Fig. 4(a), it becomes evident that as the length of the patch slot is reduced, the intensity of the first resonance weakens and shifts towards lower frequency levels. Concurrently, the second resonance becomes more pronounced in this scenario. Turning attention to Fig. 4(b), the response of the resonances in relation to changes in the ground slot width is presented. Notably, an increase in the width of the slot leads to a notable outcome: the second resonance at 38 GHz becomes narrower. Furthermore, a noteworthy phenomenon occurs with the first resonance: as the slot width widens, it transforms into a dual-band response. This transformation ultimately results in the complete disappearance of the initial resonance at 28 GHz.

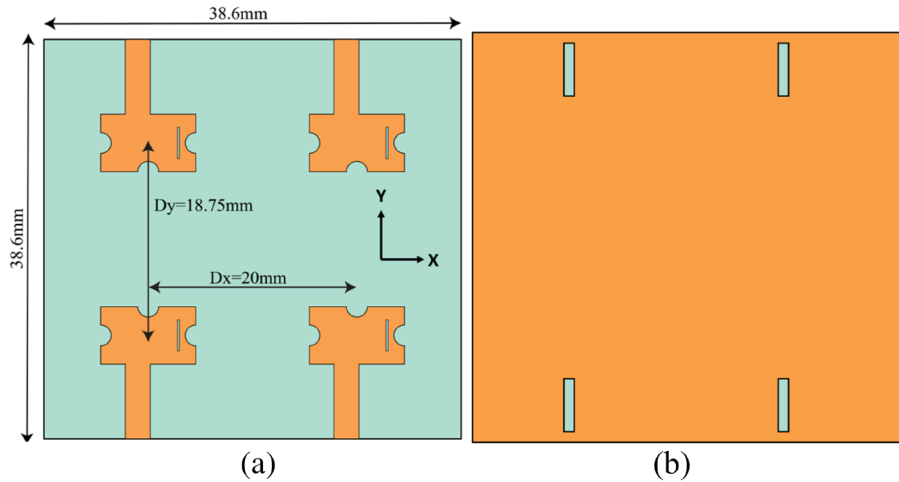
## 2.2 Four Element MIMO Antenna

After designing a single antenna element, a four-element MIMO antenna system is designed using the polarization diversity technique, as shown in Fig. 5. In MIMO configuration, the dimensions of the single antenna element remain the same, as shown in Fig. 1.

In MIMO configuration, the board size is increased to 38.6 mm × 38.6 mm. For better mutual coupling, a gap of about 20 mm is set between adjacent antenna elements, and for face-to-face elements, it is equal to 18.75 mm, as shown in Fig. 5. The proposed MIMO antenna is designed in CST Microwave Studio. Figure 6 displays the distribution of surface currents, showcasing minimal interference among radiating elements, which signifies the antenna's favorable isolation characteristics. This reduced interference is attributed to the increased separation between radiating elements. To improve isolation further, the MIMO system could be designed with antennas placed closer together, supplemented by an isolating structure. The fabricated prototype of the proposed MIMO antenna is shown in Fig. 7. The S-parameters are measured using Rhode & Schwarz's (R&S) Vector Network Analyzer (VNA) ZVA67 in the frequency range of 25–45 GHz.



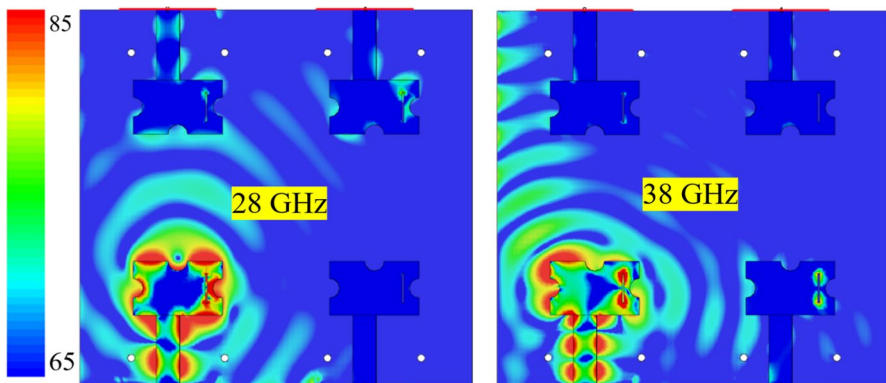
**Fig. 4** Effect of (a) patch slot length and (b) ground slot width on patch antenna performance



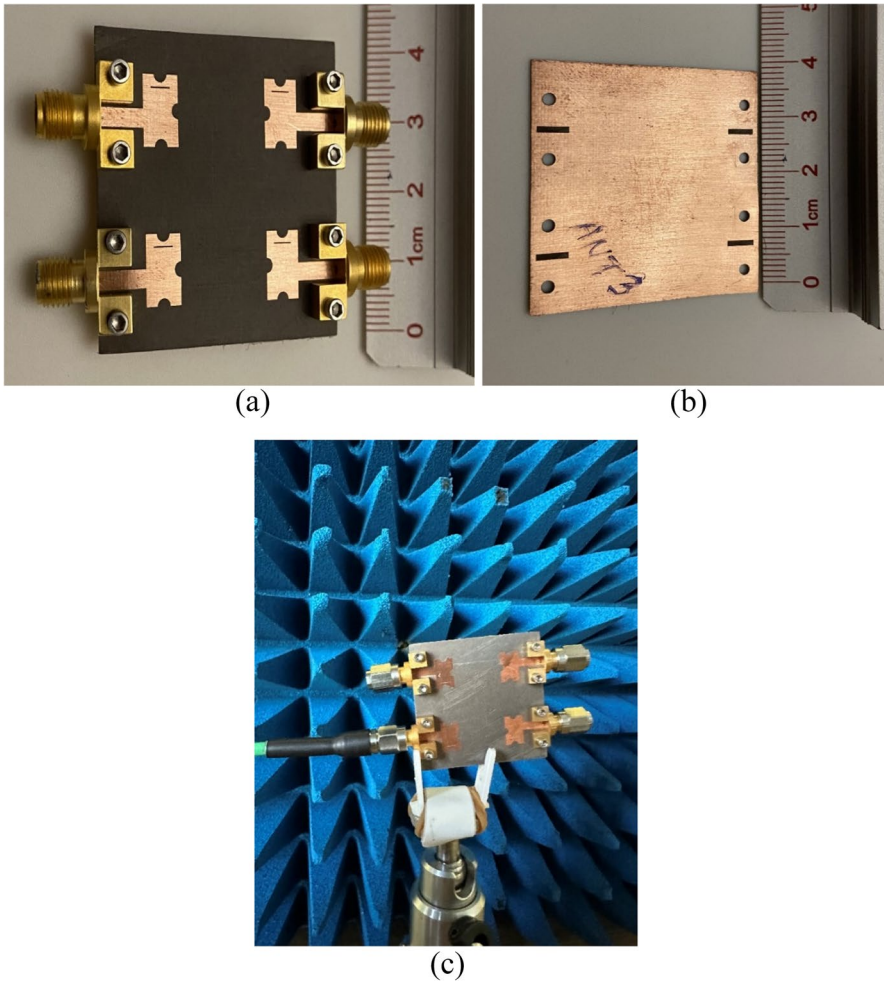
**Fig. 5** Proposed dual-band MIMO antenna configuration

Figure 8 shows the simulated and measured reflection coefficient ( $S_{11}$ ) response of the proposed MIMO antenna. It is observed that the MIMO elements are resonating well for the bands of interest. Due to symmetry, only the characteristics of two antenna elements are presented here. In the case of MIMO configuration, the impedance bandwidth at both bands is noted to be 3 GHz (27–30 GHz) and 5.46 GHz (35.54–41 GHz), as shown in Fig. 8. The measured  $S_{11}$  response is also shown in Fig. 8, and it is observed that the simulated and measured results are well in agreement. The discrepancies between the results may arise due to connector losses, fabrication intolerances, and scattering environment effects.

On the other hand, the isolation performance of the proposed MIMO antenna in terms of simulation and measurements is shown in Fig. 9. From both results, shown in Figs. 9(a) and 9(b), it is observed that the isolation between the antenna elements is  $> 15$  dB for the 28 GHz frequency band, while the isolation for the 38 GHz



**Fig. 6** Surface Currents of MIMO Configuration



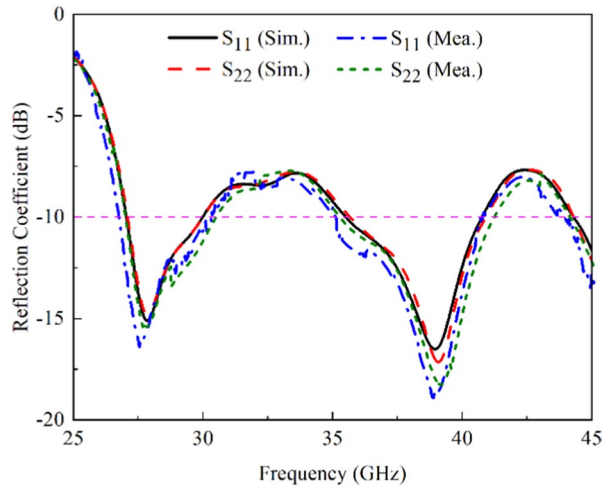
**Fig. 7** Fabricated prototype of proposed dual-band MIMO antenna. **(a)** Front **(b)** Back **(c)** Measurement Setup

frequency band is observed to be  $> 25$  dB. The simulated and measured efficiency at both resonances of 28 and 38 GHz is found to be greater than 80% as seen in Fig. 10. The peak efficiency (simulated) is notes to be 90.5% at 28 GHz. These values shos that the proposed antenna system is highly efficient. This indicates that the designed MIMO antenna can be used in devices where dual-band characteristics with low mutual coupling are required. The far-field radiation characteristics of the proposed MIMO antenna for  $xy$ - and  $zx$ -planes are shown in Fig. 11 and 3D radiation patterns are shown in Fig. 12. Here, the radiation characteristics of Ant 1 and Ant 2 are presented.

The radiation patterns are plotted for the 28 and 38 GHz frequency bands. From the figures, it is observed that the antenna offers directional characteristics for the



**Fig. 8** Simulated and measured reflection coefficient response of the proposed dual-band MIMO antenna



xy-plane. For Ant 1, the main beam is directed towards 90 degrees, while for Ant 2, it is directed towards 180 degrees. Furthermore, for the zx-plane, broadside radiation patterns are observed. It is also observed from Figs. 11 and 12 that Ant 1 and Ant 2 offer pattern diversity for both operating bands. Therefore, the presented results further justify the performance of the designed MIMO antenna. From the radiation pattern plots, one can also observe that the single antenna element offers a gain of 7.4 and 7.5 dBi at 28 and 38 GHz, respectively.

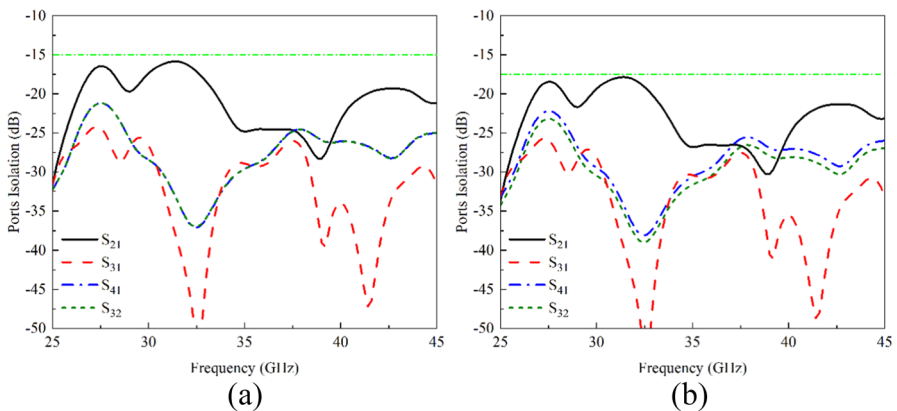


**Fig. 9** (a) Simulated and (b) measured isolation performance of the proposed dual-band MIMO antenna

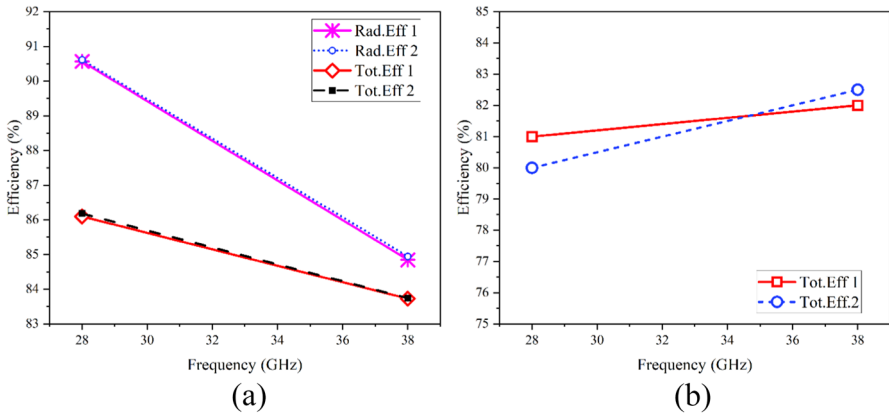


**Fig. 10** (a) Simulated Radiation and Total Efficiency (b) Measured Total Efficiency

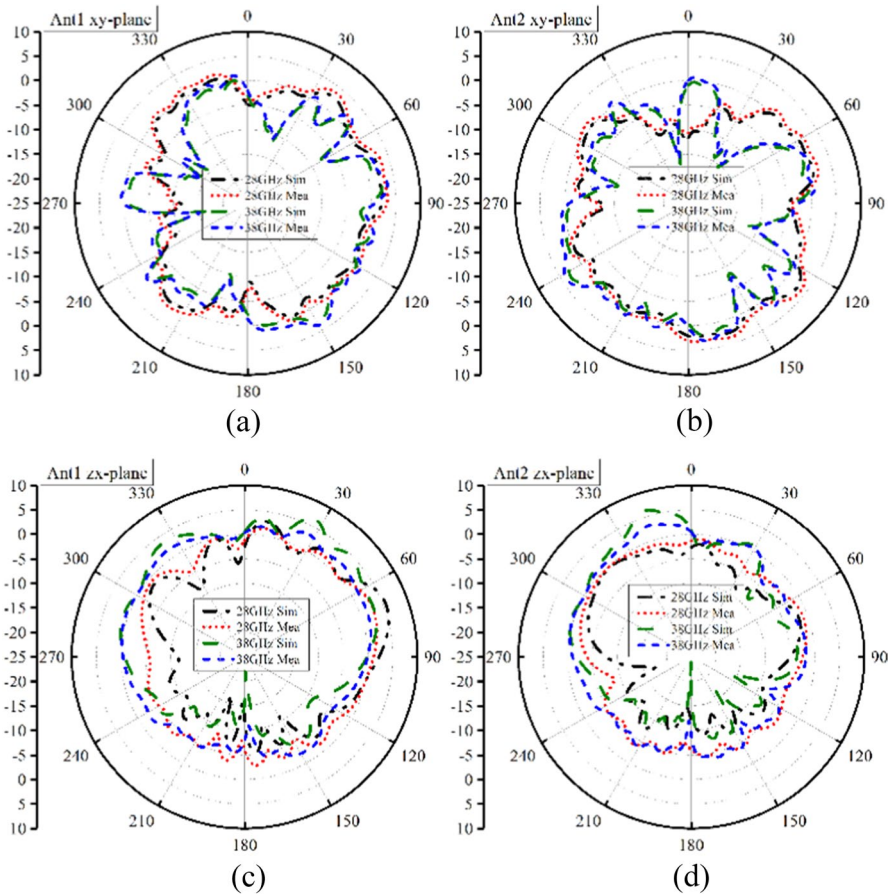


**Fig. 11** Far-field radiation characteristics of the proposed dual-band antenna for (a) xy-plane Ant 1 (b) xy-plane Ant 2. (c) zx-plane Ant 1 (d) zx-plane Ant 2

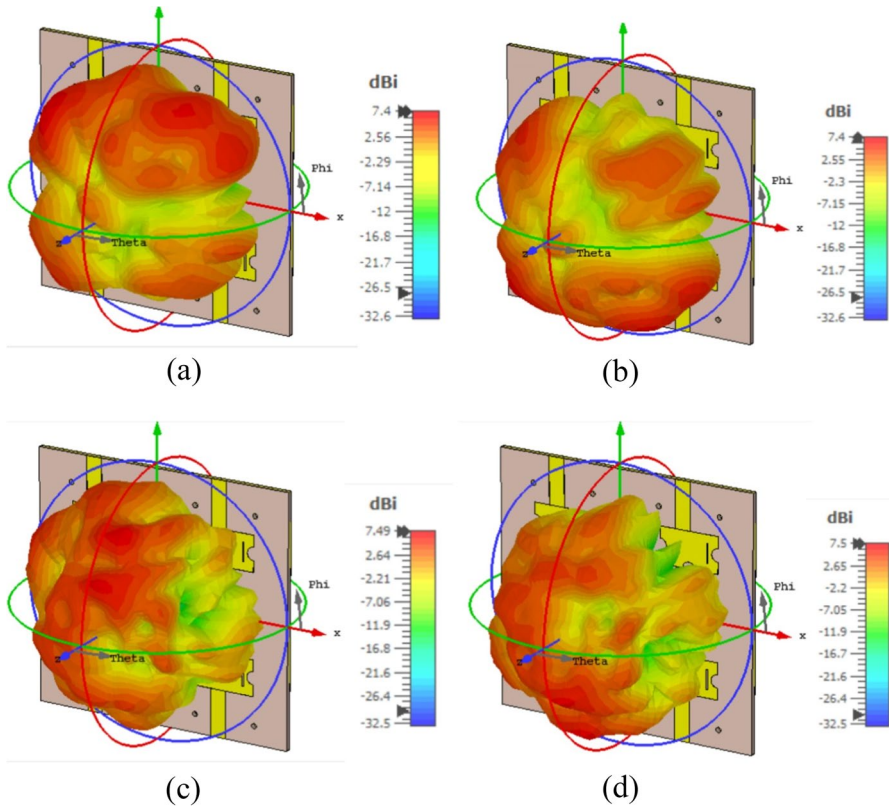


**Fig. 12** 3D Far-field radiation characteristics of the proposed dual-band antenna (a) Ant 1 28 GHz (b) Ant 2 28 GHz (c) Ant 1 38 GHz (d) Ant 2 38 GHz

### 2.3 MIMO Performance Parameters

In order to evaluate MIMO performance of the proposed system, several MIMO performance parameters studies have been conducted. MIMO parameters are essential to analyze antenna performance in real time environments [24–26]. The parameters included Mean Effective Gain (MEG), Channel Capacity Loss (CCL), Envelope Correlation Coefficient (ECC) and Diversity Gain (DG). The abovementioned MIMO parameters are conducted using method described in [27, 28]. The ECC, TARC, CCL and DG characteristics of the proposed MIMO antenna are shown in Fig. 13 while MEG is shown in Table 1. The ECC is calculated using the S-parameter characteristics using Eq. (1).

$$ECC = \frac{|S_{ii} * S_{ij} + S_{ji} * S_{jj}|^2}{(1 - |S_{ii}|^2 - S_{ij}^2)(1 - |S_{ji}|^2 - S_{jj}^2)} \tag{1}$$

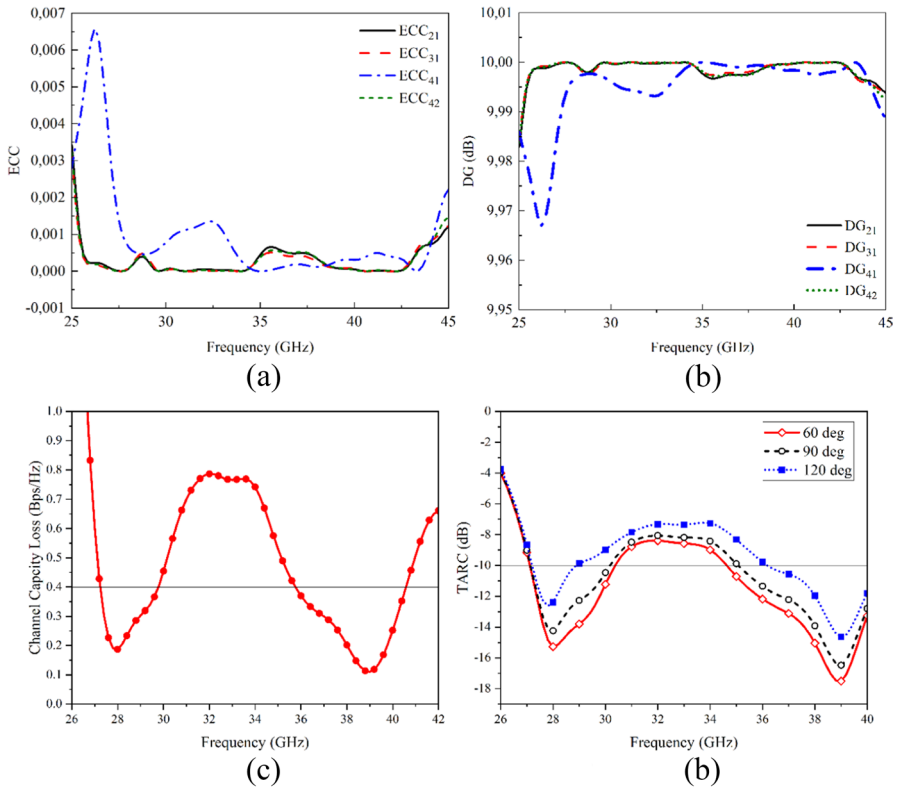


**Fig. 13** (a) ECC and (b) DG (c) CCL and (d) TARC of the proposed dual-band MIMO antenna

It is observed that the value of the ECC is approximately equal to zero, as shown in Fig. 13(a). On the other hand, the DG value is calculated using Eq. (2) for the bands of interest is equal to approximately 10 dB (see Fig. 13b). The TARC is also noted to be less than 10 dB at desired band of interest and CCL is observed less than 0.4.

$$DG = 10\sqrt{1 - ECC^2} \tag{2}$$

The proposed MIMO antenna performance metrics, as presented in Table 2, are compared with the state-of-the-art structures reported in the recent literature. The comparison is arranged in terms of the antenna type, size, operating frequency, bandwidth, isolation, gain, and the MIMO performance parameters, i.e., ECC and DG.

**Table 1** MEG of proposed MIMO antenna system

Frequency (GHz)	MEG 1	MEG 2	MEG 3	MEG 4
28	-3.88	-4.22	4.31	-3.90
38	-4.66	-4.01	-3.86	4.17

**Table 2** Comparison of proposed MIMO antenna with previously published literature

REF	ANTENNA TYPE	SIZE (MM <sup>3</sup> )	FREQ. (GHZ)	B. W (GHZ)	GAIN (DBI)	DG (DB)	ECC	ISOLA-TION (DB)
[17]	Parasitic Element MIMO Antenna	28×28×0.79	28/38	4/5	9/6.5	9.96	0.005	30
[18]	Modified Circular Patch MIMO Antenna	30×30×1.575	28	4	7	9.96	0.02	25
[19]	Microstrip antenna	19.4×13×0.254	30	2	8	9.98	0.01	36
[20]	Four-element MIMO antenna with decoupling line	13.75×13.75×0.787	35	4	3	9.6	0.04	30
[21]	Circular patch with DGS	30×30×1.575	28/38	3	5.2	9.99	0.0001	30
[22]	T-shape slotted antenna	110×55×0.508	28/38	3	7.8/8.2	N/A	0.002	28
[23]	Multilayer DRA	25×15×1	28/38	5	7	9.98	0.007	27
PROP	Modified rectangular patch	38.6×38.6×0.787	28/38	2.52/6.5	7.4/7.5	9.99	0.0001	15/25

### 3 Conclusion

A dual-band, four-element MIMO antenna design is presented for mmWave 5G communication systems. The single element of the MIMO configuration consists of a modified rectangular patch element, while the back side consists of a slot-loaded full ground plane. It is observed from the presented results that the single antenna element offers an impedance bandwidth of 2.52 GHz ranging from 26.32 to 28.84 GHz, and 7.5 GHz varies in the range of 34–41.5 GHz. After that, a MIMO antenna system is designed and fabricated. A pattern diversity configuration is utilized for the design of MIMO antennas. The MIMO antenna system offers an impedance bandwidth of 3 GHz (27–30 GHz) and 5.46 GHz (35.54–41 GHz) with a peak realized gain of 7.4 dBi and 7.5 dBi, respectively. The proposed system is novel in terms of wide bandwidth characteristics using full ground plane, directional patterns and high achieved gain as compared to printed monopole antennas which offer low gain with wideband characteristics and narrowband patch antenna structures. In addition, the isolation between the antenna elements is noted to be > 15 dB for the 28 GHz frequency band, while for the 38 GHz frequency band, the isolation is observed to be > 25 dB. Moreover, the MIMO parameter values are within acceptable limits. According to the presented results, one can conclude that the designed dual-band MIMO antenna can be considered a valuable candidate for existing or future ka band 5G communication systems.

**Acknowledgements** The authors would like to acknowledge the support of Prince Sultan University, Riyadh, Saudi Arabia for providing funding for this article.

**Author Contributions** “Conceptualization, W.T.S., S.H.K. and M.M.; methodology, S.H.K.; D.A.S.; software, W.T.S., S.H.K., M.M. and D.A.S.; validation, S.H.K., M.M. and D.A.S.; formal analysis, D.A.S., H.S.S., D.A.; investigation, S.H.K., and D.A.S.; resources, M.M., D.A.S., and H.S.S.; writing—original draft preparation, W.T.S., S.H.K.; writing—review and editing, W.T.S., S.H.K., D.A.S., D.A.; supervision, H.S.S., and D.A.” All authors have read and agreed to the published version of the manuscript.

**Funding** Open Access funding provided by Universidad Pública de Navarra.

**Data Availability** All data generated or analyzed during this study is included in this article.

#### Declarations

All of the figures, materials, and data within the manuscript are original and owned by authors.

**Ethical Approval** Not applicable.

**Competing Interests** The authors declare no competing interests.

**Open Access** This article is licensed under a Creative Commons Attribution 4.0 International License, which permits use, sharing, adaptation, distribution and reproduction in any medium or format, as long as you give appropriate credit to the original author(s) and the source, provide a link to the Creative Commons licence, and indicate if changes were made. The images or other third party material in this article are included in the article's Creative Commons licence, unless indicated otherwise in a credit line to the material. If material is not included in the article's Creative Commons licence and your intended use is not permitted by statutory regulation or exceeds the permitted use, you will need to obtain permission

directly from the copyright holder. To view a copy of this licence, visit <http://creativecommons.org/licenses/by/4.0/>.

## References






1. X. Lin, "An overview of 5G advanced evolution in 3GPP," *IEEE Communications Standards Magazine*, vol. 18, no. 3, pp. 77–83, 2022.
2. J. Li et al., "Mobility Support for Millimeter Wave Communications: Opportunities and Challenges," *IEEE Communications Surveys & Tutorials*, vol. 24, no. 3, pp. 1816–1842, 2022.
3. T. Islam, E. M. Ali, W. A. Awan, M. S. Alzaidi, T. A. Alghamdi, and M. Alathbah, "A parasitic patch loaded staircase shaped uwb mimo antenna having notch band for wlan applications," *Heliyon*, vol. 10, no. 1, p. e23711, 2024.
4. Y. Jiang, S. Liu, M. Li, N. Zhao, and M. Wu, "A new adaptive co-site broadband interference cancellation method with auxiliary channel," *Digital Communications and Networks*, 2022
5. W.A. Awan, M. Soruri, M. Alibakhshikenari, and E. Limiti, "On-demand frequency switchable antenna array operating at 24.8 and 28 GHz for 5G high-gain sensors applications," *Progress In Electromagnetics Research M*, Vol. 108, pp. 163–173, 2022.
6. Jung, J., Awan, W. A., Choi, D., Lee, J., Hussain, N., & Kim, N. (2023). Design of high-gain and low-mutual-coupling multiple-input–multiple-output antennas based on prs for 28 GHz applications. *Electronics*, 12(20), 4286.
7. Jiang, Y., & Li, X. (2022). Broadband cancellation method in an adaptive co-site interference cancellation system. *International journal of electronics*, 109(5), 854–874.
8. M. Hussain, S. Iffat Naqvi, W. Abbas Awan, W. Abd Ellatif Ali, E. Mousa Ali, S. Khan, and M. Alibakhshikenari, "Simple wideband extended aperture antenna- inspired circular patch for v-band communication systems," *AEU - International Journal of Electronics and Communications*, vol. 144, p. 154061, 2022.
9. Cao, K., Ding, H., Li, W., Lv, L., Gao, M., Gong, F., & Wang, B. (2022). On the ergodic secrecy capacity of intelligent reflecting surface aided wireless powered communication systems. *IEEE wireless communications letters*, 11(11), 2275–2279.
10. Zhang, Y., Zhao, P., Lu, Q., Zhang, Y., Lei, H., Yu, C., ... & Yu, J. (2023). Functional additive manufacturing of large-size metastructure with efficient electromagnetic absorption and mechanical adaptation. *Composites Part A: Applied Science and Manufacturing*, 173, 107652.
11. Q. Wang et al., "Interval-Based Tolerance Analysis Method for Petal Reflector Antenna With Random Surface and Deployment Errors," in *IEEE Transactions on Antennas and Propagation*, vol. 71, no. 11, pp. 8556–8569, Nov. 2023. <https://doi.org/10.1109/TAP.2023.3314097>.
12. Awan, W. A., Hussain, N., Park, S. G., & Kim, N. (2024). Intelligent metasurface based antenna with pattern and beam reconfigurability for internet of things applications. *Alexandria Engineering Journal*, 92, 50–62
13. S. I. Naqvi, N. Hussain, A. Iqbal, M. Rahman, M. Forsat, S. Mirjavadi, and Y. Amin, "Integrated LTE and millimeter-wave 5G MIMO antenna system for 4G/5G wireless terminals," *Sensors*, vol. 20, no. 14, article no. 3926, 2020.
14. S. I. Naqvi, A. H. Naqvi, F. Arshad, M. A. Riaz, M. A. Azam, M. S. Khan, Y. Amin, J. Loo, and H. Tenhunen, "An integrated antenna system for 4G and millimeter-wave 5G future handheld devices," *IEEE Access*, vol. 7, pp. 116555–116566, 2019.
15. A. Zaidi, W. A. Awan, A. Baghdad, N. Hussain, A. Ballouk and A. Badri, "Compact Size T-Shaped Patch Antenna for E-Band Applications," 2019 International Conference on Wireless Networks and Mobile Communications (WINCOM), Fez, Morocco, 2019, pp. 1–3, <https://doi.org/10.1109/WINCOM47513.2019.8942527>.
16. M. N. Hasan, S. Bashir, and S. Chu, "Dual band omnidirectional millimeter wave antenna for 5G communications," *Journal of Electromagnetic Waves and Applications*, vol. 33, no. 12, pp. 1581–1590, 2019.
17. Hussain M, Awan WA, Ali EM, Alzaidi MS, Alsharaf M, Elkamchouchi DH, Alzahrani A, Fathy Abo Sree M. Isolation Improvement of Parasitic Element-Loaded Dual-Band MIMO Antenna

- for Mm-Wave Applications. *Micromachines*. 2022; 13(11):1918. <https://doi.org/10.3390/mi13111918>
18. Hussain M, Mousa Ali E, Jarchavi SMR, Zaidi A, Najam AI, Alotaibi AA, Althobaiti A, Ghoneim SSM. Design and Characterization of Compact Broadband Antenna and Its MIMO Configuration for 28 GHz 5G Applications. *Electronics*. 2022; 11(4):523. <https://doi.org/10.3390/electronics11040523>
  19. W. Wang, Y. Wu, W. Wang, and Y. Yang, "Isolation enhancement in dual-band monopole antenna for 5G applications," *IEEE Transactions on Circuits and Systems II: Express Briefs*, vol. 68, no. 6, pp. 1867-1871, 2021.
  20. J. S. Park, J. B. Ko, H. K. Kwon, B. S. Kang, B. Park, and D. Kim, "A tilted combined beam antenna for 5G communications using a 28-GHz band," *IEEE Antennas and Wireless Propagation Letters*, vol. 15, pp. 1685-1688, 2016.
  21. M. Khalid, S. I. Naqvi, N. Hussain, M. Rahman, S. S. Mirjavadi, M. J. Khan, and Y. Amin, "4-Port MIMO antenna with defected ground structure for 5G millimeter wave applications," *Electronics*, vol. 9, no. 1, article no. 71, 2020.
  22. N. Yoon and C. Seo, "A 28-GHz wideband 2x2 U-slot patch array antenna," *Journal of Electromagnetic Engineering and Science*, vol. 17, no. 3, pp. 133-137, 2017.
  23. P. Liu, X. W. Zhu, Y. Zhang, X. Wang, C. Yang, Z.H. Jiang, "Patch antenna loaded with paired shorting pins and H-shaped slot for 28/38 GHz dual-band MIMO applications." *IEEE Access*, vol. 8, pp. 23705-23712, 2020.
  24. M. Dai, G. Sun, H. Yu, and D. Niyato, "Maximize the long-term average revenue of network slice provider via admission control among heterogeneous slices," *IEEE/ACM Transactions on Networking*, vol. 32, no. 1, pp. 745–760, 2024
  25. Huang, X. L., Zhou, L., Völkel, M., Hagelauer, A., Mao, J. F., & Weigel, R. (2018). Design of a novel quarter-mode substrate-integrated waveguide filter with multiple transmission zeros and higher mode suppressions. *IEEE Transactions on Microwave Theory and Techniques*, 66(12), 5573-5584.
  26. Huang, X., Zhang, X., Zhou, L., Xu, J. X., & Mao, J. F. (2022). Low-loss self-packaged Ka-band LTCC filter using artificial multimode SIW resonator. *IEEE Transactions on Circuits and Systems II: Express Briefs*, 70(2), 451-455.
  27. Y. Zhang, W. Yang, Q. Xue, J. Huang, W. Che, "Broadband dual-polarized differential-fed filtering antenna array for 5G millimeter-wave applications. " *IEEE Transactions on Antennas and Propagation*, Vol. 70, pp. 1989-1998, 2022.
  28. W. A. Awan, E. M. Ali, M. S. Alzaidi, D. H. Elkamchouchi, F. N. Alsunaydih, F. Alsaleem, and K. Alhassoon, "Enhancing isolation performance of tilted beam mimo antenna for short-range millimeter wave applications," *Heliyon*, vol. 9, no. 9, p. e19985, 2023

**Publisher's Note** Springer Nature remains neutral with regard to jurisdictional claims in published maps and institutional affiliations.



## Authors and Affiliations

Waleed Tariq Sethi<sup>1</sup> · Saad Hassan Kiani<sup>2</sup>  · Mehre E. Munir<sup>3</sup>  ·  
Daniyal Ali Sehrai<sup>4,6</sup>  · Huseyin şerif savci<sup>2</sup>  · Dawar Awan<sup>5</sup> 

✉ Saad Hassan Kiani  
iam.kiani91@gmail.com

✉ Daniyal Ali Sehrai  
daniyalali.sehrai@unavarra.es

- <sup>1</sup> Faculty of Electrical Engineering, Ghulam Ishaq Khan Institute of Engineering Sciences and Technology, Swabi 23640, Khyber Pakhtunkhwa, Pakistan
- <sup>2</sup> Electrical and Electronics Engineering Department, Faculty of Engineering and Natural Sciences, Istanbul, Medipol University, 34810 Istanbul, Turkey
- <sup>3</sup> Smart Systems Engineering Laboratory, College of Engineering, Prince Sultan University, 11586 Riyadh, Saudi Arabia
- <sup>4</sup> Department of Electric, Electronic and Communication Engineering, Public University of Navarre (UPNA), Arrosadia Campus, 31006 Pamplona, Spain
- <sup>5</sup> Department Electrical Technology, University of Technology, Nowshera, Pakistan
- <sup>6</sup> CRUE-CSIC Alliance, Public University of Navarre (UPNA), Pamplona, Spain